The Canadian Mineralogist
Vol. 44, pp. 1357-1366 (2006)

RAMAN SPECTROSCOPIC STUDY OF VARIABLY RECRYSTALLIZED METAMICT ZIRCON FROM AMPHIBOLITE-FACIES METAGRANITES, SERBO-MACEDONIAN MASSIF, BULGARIA

ROSITSA TITORENKOVA[§]

Central Laboratory of Mineralogy and Crystallography, Bulgarian Academy of Sciences, Acad. G. Bonchev Street 107, 1113 Sofia, Bulgaria

BORIANA MIHAILOVA

Mineralogisch-Petrographisches Institut, University of Hamburg, Grindelallee 48, D–20146 Hamburg. Germany

LUDMIL KONSTANTINOV

Central Laboratory of Mineralogy and Crystallography, Bulgarian Academy of Sciences, Acad. G. Bonchev Street 107, 1113 Sofia, Bulgaria

ABSTRACT

We investigated zircon from high-grade metagranites of the Serbo-Macedonian Massif, in Bulgaria, by cathodoluminescence (CL), back-scattered-electron imaging, electron-microprobe analysis, and Raman microspectroscopy. The structural state in various zones was assessed using: (i) the position and width of the Raman peak near 1008 cm^{-1}, (ii) the relative Raman intensity of the symmetrical and anti-symmetrical SiO_4 modes, (iii) the width of the peaks near 357 and 439 cm^{-1}, and (iv) the occurrence of extra Raman scattering near 162, 509, 635 and 785 cm^{-1}. The analyzed zones are divided into two main groups: (A) areas with a well-resolved Raman peak near 1008 cm^{-1}, and (B) areas with a very weak Raman scattering near 1008 cm^{-1}. Group B can be classified into two subgroups: (B-i) dark zones in CL images, with a high concentration of uranium (up to 7000 ppm), and (B-ii) outermost bright zones in CL images with a concentration of U lower than that in the inner areas and commonly below the detection limit. The samples from group A contain uranium at intermediate levels of concentration (~350–2000 ppm), and exhibit a linear correlation between the width and the position of the peak near 1008 cm^{-1}. The relatively narrow width of this peak provides evidence of structural recovery due to annealing of accumulated radiation-induced damage. In zircon from equigranular metagranites, which are relatively less deformed and migmatized, three types of spatial regions are observed: the least-damaged regions with a structure altered mainly by point defects, moderately damaged regions characterized by faults with translational symmetry, and heavily damaged zircon with additional medium-range disorder involving changes in the mutual orientation of the cation–oxygen polyhedra and in their connectivity. The zircon separated from more deformed and strongly migmatized rocks is relatively homogeneous in its texture and chemical composition, and its structure consists of incipient grains of zircon.

Keywords: zircon, metamictization, Raman spectroscopy, cathodoluminescence, back-scattered-electron imagery, metagranite, Serbo-Macedonian Massif, Bulgaria.

SOMMAIRE

Nous avons étudié le zircon provenant de métagranites fortement recristallisés du massif Serbo-Macédonien, en Bulgarie, par cathodoluminescence (CL), analyses d'images avec électrons rétrodiffusés, analyses par microsonde électronique, et micro-spectroscopie de Raman. L'état structural des diverses zones a été évalué selon (i) la position et la largeur du pic de Raman près de 1008 cm^{-1}, (ii) l'intensité relative des modes SiO_4 symétrique et anti-symétrique du spectre de Raman, (iii) la largeur des pics près de 357 et 439 cm^{-1}, et (iv) la présence de dispersion de Raman supplémentaire près de 162, 509, 635 et 785 cm^{-1}. Les zones analysées sont divisées en deux groupes principaux: (A) régions ayant un pic Raman près de 1008 cm^{-1} bien résolu, et (B) régions montrant une très faible dispersion de Raman près du pic à 1008 cm^{-1}. On peut diviser le groupe B en deux sous-groupes: (B-i) zones sombres dans les images CL, avec une forte concentration d'uranium (jusqu'à 7000 ppm), et (B-ii) zones externes claires dans les images CL, avec une concentration d'uranium plus faible que dans les zones internes et généralement en dessous du seuil de détection. Les échantillons du groupe A contiennent de l'uranium à des niveaux intermédiaires de concentration (~350–2000 ppm), et montrent une corrélation linéaire entre la largeur et la position du pic près de 1008 cm^{-1}. L'étroitesse de ce

§ *E-mail address*: rosititorenkova@dir.bg

pic semble indiquer qu'il y a eu restauration structurale par recuit du dommage accumulé à cause de la radiation. Dans le zircon des métagranites équigranulaires, qui sont relativement moins déformés et migmatisés, nous observons trois types de domaines: les régions faiblement endommagées, avec une structure surtout modifiée par défauts ponctuels, les régions modérément endommagées, dans lesquelles les failles ont une symétrie translationnelle, et les régions fortement endommagées, avec par surcroit un désordre à l'échelle moyenne impliquant des changements de l'orientation mutuelle des polyèdres à liaisons cation–oxygène et leur connectivité. Le zircon provenant des roches plus fortement déformées et migmatisées est relativement homogène dans sa texture et sa composition chimique, et sa structure contient des germes de zircon.

(Traduit par la Rédaction)

Mots-clés: zircon, metamictisation, spectroscopie de Raman, cathodoluminescence, analyses d'images avec électrons rétrodiffusés, métagranite, massif Serbo-Macédonien, Bulgarie.

Introduction

Zircon ($ZrSiO_4$) belongs to the group of accessory minerals that may become metamict, *i.e.*, characterized with a high degree of structural disorder and a coexistence of defect-rich crystalline domains and amorphous regions on a micrometric to submicrometric scale. The incorporation of radionuclides in zircon results in α-decay events and the formation of daughter products, inciting transformations to a disordered state (Holland & Gottfried 1955). Depending on the dose of radiation, various structural modifications may occur: generation of point defects, formation of metastable phases, polymerization of SiO_4 tetrahedra, appearance of ZrO_2 as a high-temperature phase, and even a complete amorphization of the zircon (Ewing *et al*. 2000, Trachenko *et al*. 2002). However, several complementary processes that take place over geological times have influenced the final state of natural zircon, namely radiation-induced metamictization, annealing-induced structural recovery, recrystallization, and secondary fluid-induced alteration, most important in metamorphic rocks. Thus, the study of natural zircon is essential for at least two reasons: (i) age dating and interpretation of the thermal history of zircon (Nasdala *et al*. 2001a, Geisler & Pidgeon 2002), and (ii) immobilization of radioactive waste and related environmental contamination, as zircon can be utilized as a host mineral for disposal of actinides (Ewing *et al*. 1995).

Our aim in this study is to document the variations in the local structure of naturally inhomogeneous zircon and to compare the structural peculiarities with textural features and the distribution of radioactive elements. For this purpose, we have applied micro Raman spectroscopy to estimate the degree of structural modification in different spatial regions in samples of zircon from metagranites with various degrees of deformation and migmatization and from melanocratic enclaves.

Background Information

The structure of zircon has been extensively investigated by various techniques, such as cathodoluminescence (CL) and back-scattered-electron (BSE) imaging, infrared and Raman spectroscopy, X-ray and electron diffraction, high-resolution transmission electron microscopy and sensitive high-mass-resolution ion microprobe (Ewing *et al*. 2003, Nasdala *et al*. 2003, and references therein). Raman spectroscopy is a versatile and powerful experimental tool for structural investigations, and it has also been applied to zircon. The position and the width of the peak near 1008 cm^{-1}, arising from the $B_{1g}[\nu_3(SiO_4)]$ phonon mode, are very sensitive spectral parameters to the degree of structural damage of zircon. Nasdala *et al*. (1995) has proposed to use the full width at half maximum (FWHM) of this peak for quantitative analysis of the degree of metamictization of zircon and, further, to estimate the annealing history of unknown samples *via* the dependence of FWHM on the radioactive α-dose (Nasdala *et al*. 2001a, Palenik *et al*. 2003). However, Geisler & Pidgeon (2002) have stated that phonon-confinement effects may also contribute to the spectral parameters of the $B_{1g}[\nu_3(SiO_4)]$ mode, *i.e.*, the α-dose is not the only factor determining the FWHM. The authors have suggested that the dependence of wavenumber *versus* FWHM of the $B_{1g}[\nu_3(SiO_4)]$ mode as a more appropriate way to estimate the effects of geological events.

Zhang *et al*. (2000) have performed a series of dry-annealing experiments. Their Raman spectroscopic study reveals that depending on the initial stage of damage, the zircon structure undergoes diverse modifications upon heating. The recrystallization of heavily metamict zircon passes through an intermediate stage of decomposition into ZrO_2 and SiO_2 phases, whereas partially metamict zircon recovers directly at relatively low temperatures. In addition, Geisler & Pidgeon (2001), and Nasdala *et al*. (2002) showed that both the integrated CL intensity and the panchromatic CL images of natural zircon correlate well with the radiation-induced degree of structural disorder, as determined by Raman spectroscopy. Further, the stability of zircon under hydrothermal conditions has been studied experimentally using vibrational spectroscopy, but the type of hydrous species and their role in the metamictization and recrystallization processes are still not clarified (Nasdala *et al*. 2001b, 2003, Geisler *et al*. 2003a, b).

Materials and Methods

In this study, fifteen crystals of zircon were analyzed at thirty-nine different points. The zircon samples were separated from metagranite samples recrystallized under amphibolite-facies conditions (650°C, 6–7 kbar) and exposed in the Ograzhden Mountains, Serbo-Macedonian massif, Bulgaria. The Ograzhdenian block of the Serbo-Macedonian Massif consists of amphibolite-facies metamorphic rocks belonging to the Ograzhdenian Supergroup, Maleshevska Group. Two types of metagranite are distinguished: one has an equigranular texture, and the other is porphyritic, with K-feldspar phenocrysts. K-feldspar-phyric metagranites are coarse- to medium-grained, selectively partially melted (migmatized), with an augen, augen-layered or layered structure. Equigranular metagranites are relatively less deformed and migmatized, and reveal well-preserved magmatic characteristics, such as microgranular enclaves and foliated aplitic and pegmatitic dikes. Relict magmatic minerals are rarely preserved. The chemical composition of both varieties of metagranite corresponds to an S-type protolith. The zircon we investigated comes from equigranular and porphyritic metagranites, as well as from microgranular enclaves. The age of granite intrusion was determined by thermal ionization mass spectrometry on single grains of zircon at about 460 Ma (Titorenkova *et al*. 2003).

Back-scattered-electron (BSE) images were obtained using an Oxford Instrument Stereoscan 250 Mk3, operating at an accelerating voltage of 15 kV and a beam current of 50 nA. Cathodoluminescence (CL) images were taken with a Philips SEM 515 scanning electron microscope operating at 25 kV. Selected samples of zircon were analyzed for major (Zr, Si) and trace (Hf, Y, U, P, Fe, Yb, Dy, Er, Th, Al) elements with an automated JEOL 8600 SEMQ superprobe equipped with five wavelength-dispersive spectrometers. The acceleration voltage was 20 kV at a beam current of 20 nA and a beam diameter of 1 μm. Counting times of single-spot analyses were 15 s for Zr$L\alpha$, 20 s for Si$K\alpha$, 20 s for Fe$K\alpha$ and Al$K\alpha$, 30 s for P$K\alpha$, Y$L\alpha$, Th$M\alpha$, U$M\alpha$, Hf$L\alpha$, Yb$L\alpha$, Er$L\alpha$ and Dy$L\alpha$ peaks. Synthetic glasses and natural zircon were used as standards. The detection limit for trace elements was 0.01 wt% for P, Th, U and Fe, 0.02 wt% for Hf, Er and Dy, and 0.03 wt% for Al and Yb oxides. The 2σ counting error for U was about 7.0% at 3000 ppm and 20% at 1000 ppm concentration, whereas for Th, the 2σ error was between 30% at 550 ppm and 80% at 200 ppm.

Raman spectroscopic measurements were performed at room temperature using a Horiba Jobin–Yvon T64 000 triple monochromator system equipped with a liquid N_2-cooled CCD detector and an Olympus BH2 microscope. Non-polarized spectra were collected in back-scattering geometry with a spectral resolution of 2 cm^{-1}. The diameter of the laser spot on the sample surface was approximately 1.5 μm, whereas the power of the laser beam at the sample surface was varied between 7.0 and 0.2 mW in order to assure non-destructive experimental conditions. To achieve an acceptable and effective Raman cross-section regardless of the low laser power, a laser line with a wavelength of 514.5 nm was used as incident radiation. Samples with a well-defined external morphology were selected for the Raman measurements. The zircon crystals were oriented with their *c* axis approximately perpendicular to the laser beam. Furthermore, the orientation of the crystals was adjusted to the polarization of the incident light through in-plane rotation of the sample in order to achieve maximum intensity of the Raman scattering near 1008 cm^{-1}, which is the most intense Raman signal of defect-poor zircon where the polarization of the incident light is perpendicular to the *c* axis. The experimental geometry remained unchanged during the slight shift of the sample to focus the laser spot on different spatial regions of the same grain. In all cases where extra peaks were detected (not typical of zircon), the spectra were measured also with a 488 nm excitation line in order to distinguish the possible photoluminescence-induced signals from inelastic scattering of light due to atomic vibrations. In addition, the Raman scattering in the ranges 1250–2000 and 2700–3200 cm^{-1} was examined to check for the possible artificial contribution from the epoxy resin matrix in which the zircon grains were embedded. The measured Raman spectra were subsequently corrected for the continuous luminescence-induced background using a five-degree polynomial function.

Results

Internal texture and chemical composition

Zircon from high-grade metamorphic rocks commonly exhibits a complex internal texture visible by CL and BSE microscopy (Benisek & Finger 1993, Vavra *et al*. 1999). The petrological and geochemical data show that all the metagranite samples from which the zircon grains were separated are peraluminous (an Aluminum Saturation Index between 1.02 and 1.48). This suggests a low solubility of zircon in the melt, and the existence of inherited cores. Figure 1 displays different types of inner texture of zircon. The presence of an inherited core is clearly seen in Figures 1a, b. A fine zonal growth is evident for all of the samples. However, the zoning is blurred to various extents owing to the increase in diffusion during the metamorphic processes. The rim observed in the majority of samples taken from porphyritic metagranites, which are most affected by the migmatization, may result from surface-controlled recrystallization (Fig. 1c). The origin of the texture consisting of irregularly shaped regions that overlap the growth zoning (Fig. 1d) can be related to solid-state recrystallization on a defect-enriched front (Hoskin & Black 2000), to fluid interaction on a chemical reaction

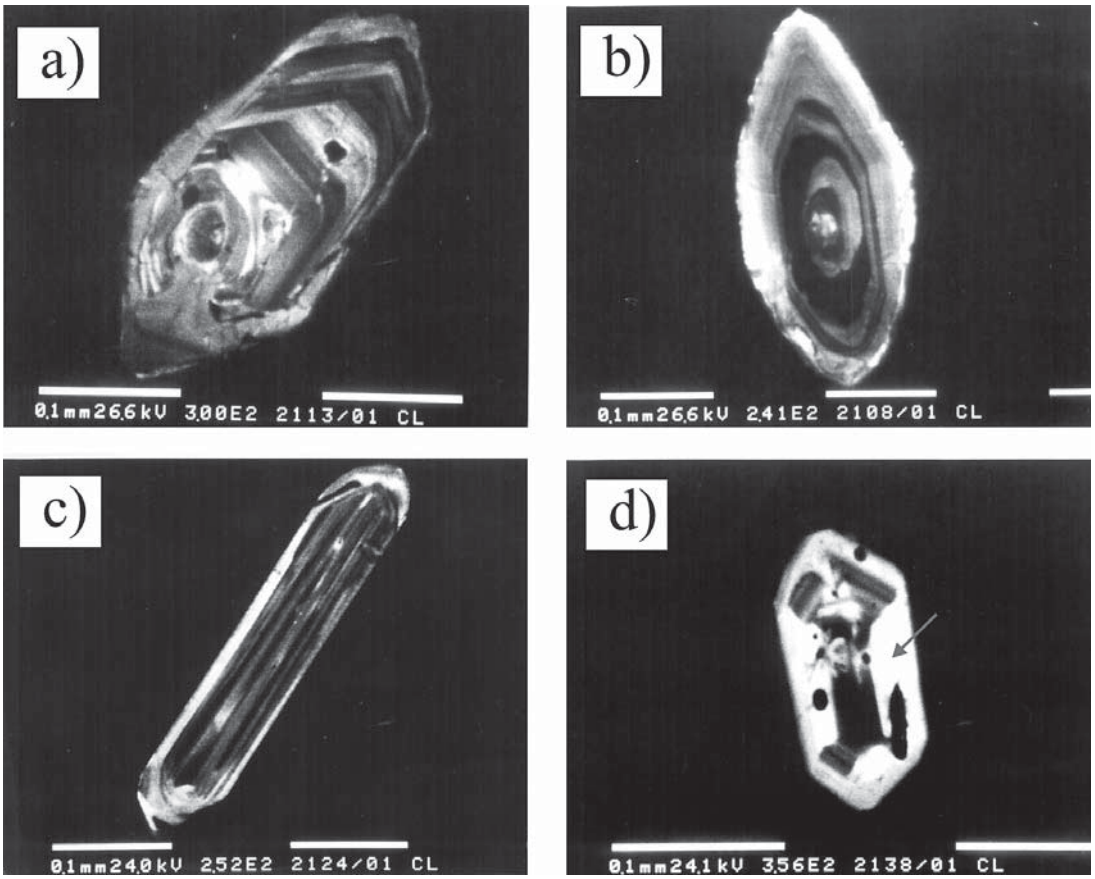

FIG. 1. CL images of zircon exhibiting an inherited core and zonal growth (a), an inherited core and blurred zoning (b), fine zonal growth and a metamorphic rim (c), and secondary stage transgressive zones, marked by the arrow (d).

front (Schaltegger *et al.* 1999) or to luminescence of REE^{3+} ions (Hanchar & Rudnik 1995). In Table 1, we summarize the chemical composition, the location in the grain, the type of host rock, the CL response of the regions studied by Raman spectroscopy, and the position and FWHM of the peak near 1008 cm^{-1} for four representative samples of zircon. The regions richest in U (up to 0.5 wt% UO_2), Y (up to 0.6 wt% Y_2O_3), Hf (up to 1.8 wt% HfO_2), and P (up to 0.5 wt% P_2O_5) were detected in the dark CL areas and are considered to be metamict. The inherited cores are characterized by a lower content of the above-listed elements: up to 0.1 wt% UO_2, 0.1–0.4 wt% Y_2O_3, 1.2–1.6 wt% HfO_2, and up to 0.3% P_2O_5, which is related to their primary origin. The irregular, featureless areas that appear bright in the CL images exhibit a low content of uranium and thorium. Usually, such areas are considered to be recrystallized zircon (Pidgeon 1992).

Raman microspectroscopy

The normal Raman-active phonon modes of zircon have been studied extensively (Dawson *et al.* 1971, Syme *et al.* 1977, Kolesov *et al.* 2001). The most intense Raman scattering appears at 1008, 439 and 357 cm^{-1}. The first two peaks have been attributed to the internal antisymmetrical stretching mode $B_{1g}[\nu_3(SiO_4)]$ and to the symmetrical bending mode of SiO_4 tetrahedra $A_{1g}[\nu_2(SiO_4)]$, respectively. The signal at 357 cm^{-1} has been inconsistently related to internal antisymmetrical bending (Dawson *et al.* 1971) and to the external rotational mode of the SiO_4 units (Syme *et al.* 1977). The latter assignment is based on experimental observation of the complete number of Raman-active modes predicted by the group-theory analysis and has been supported by further structural investigations of nonmetamict zircon (Kolesov *et al.* 2001). Thus, we assume that the peak at 357 cm^{-1} arises from the $E_g[rot(SiO_4)]$ mode.

TABLE 1. CHEMICAL COMPOSITION (in wt%), CL RESPONSE AND THE POSITION AND WIDTH OF THE RAMAN PEAK ORIGINATING FROM B_{1g} [$\nu_3(SiO_4)$] FOR DIFFERENT SPATIAL AREAS IN THE GRAINS OF ZIRCON

Sample	Area	CL	SiO_2	ZrO_2	P_2O_5	HfO_2	Y_2O_3	UO_2	ThO_2	Yb_2O_3	Er_2O_3	Dy_2O_3	FeO*	Al_2O_3	Total	Position	FWHM§
Z1a	center	high	33.1	65.5	0.09	1.28	0.19	0.03	0.05	-	0.03	-	-	-	100.3	1002.9	5.11 ± 0.1
Z1b	periphery	low	33.1	63.3	0.05	2.18	0.11	0.16	-	-	-	-	-	-	98.9	1002	8.31 ± 0.2
Z2a	center	low	32.8	64.5	0.07	1.54	-	0.10	0.09	-	0.07	0.07	0.04	-	99.4	1005.5	8.2 ± 0.2
Z2b	rim	low	32.9	64.6	-	1.98	0.24	0.54	0.05	0.08	-	-	-	-	100.4	-	-
Z2c	rim	high	33.0	62.8	0.49	1.77	0.58	0.49	0.03	0.22	0.12	0.10	0.12	0.17	99.8	-	-
Z3a	core	high	32.9	64.3	-	1.31	0.12	0.11	-	-		0.05	-	-	98.9	1004.3	8.12 ± 0.8
Z3b	zone	low	32.8	63.8	0.17	2.00	0.21	0.29	-	0.17	-	-	-	-	99.6	-	-
Z3c	zone	high	33.0	64.1	0.15	1.64	0.09	0.03	-	0.13	-	-	-	-	99.2	1002.2	7.05 ± 1.1
Z4a	center	low	32.5	64.1	0.15	1.59	0.20	0.18	-	0.05	0.06	-	-	-	98.9	1001.8**	7.48 ± 1.0
Z4b	periphery	low	32.6	64.8	0.08	1.69	0.11	0.13	-	-	0.08	0.07	-	-	99.6	1002.9**	6.18 ± 0.7

* Total Fe expressed as FeO. ** As measured with 0.02 W. § Corrected FWHM.

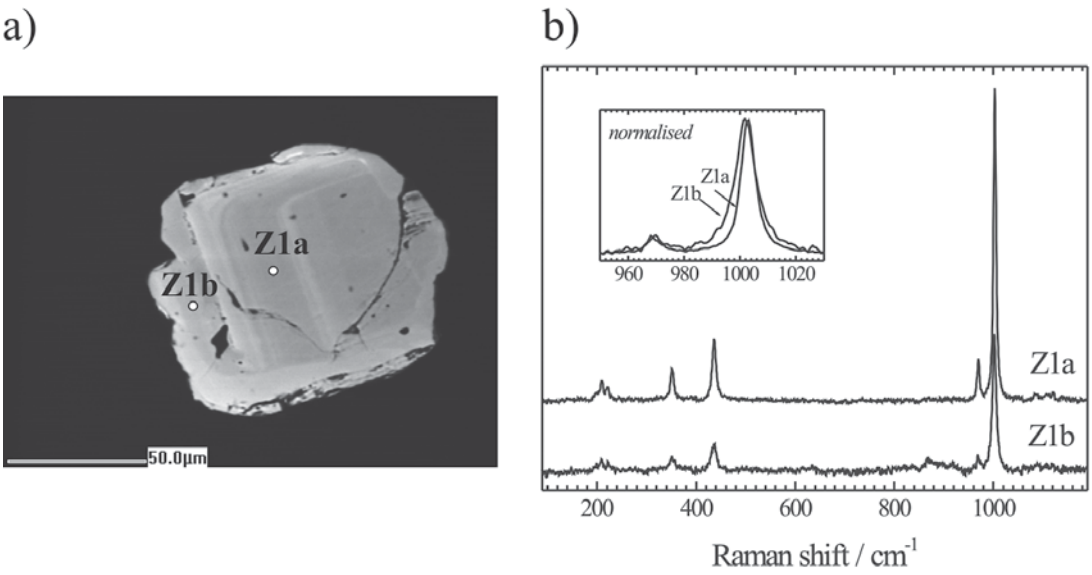

FIG. 2. BSE image of sample Z1 (a) and Raman spectra collected from the areas Z1a and Z1b (b). The insert displays the spectra normalized to the height of the peak near 1008 cm^{-1}.

Figures 2–5 illustrate four representative grains of zircon exhibiting substantially differing types of internal textures. Figure 2 shows a grain of zircon from equigranular metagranites. The magmatic zonal-growth features, barely affected by secondary post-crystallization processes, are clearly seen in the BSE image. The preserved zoning and chemical composition indicate a low rate of diffusion of impurities within this grain of zircon. The Raman spectra taken from this crystal resemble that of well-crystallized zircon, which shows that the structure has slightly been affected by radiation-decay damage. Palenik *et al*. (2003) have shown that the width of the Raman peak at 1008 cm^{-1} is proportional to the degree of disorder in zircon. As this peak is related to the $\nu_3(SiO_4)$ stretching mode, the structural disorder resulted in variations in the Si–O bond-lengths, most probably provoked by the presence of point defects. The lower wavenumber of the peak, the larger peak-

width, and the lower overall intensity of the spectrum collected from Z1b, compared to the spectrum at Z1a (Fig. 2), indicate a higher degree of metamictization in the peripheral zone than in the inner areas. On the other hand, it is known that the degree of structural damage depends on the accumulated radiation-dose, which is approximately proportional to the concentration of uranium (Palenik *et al*. 2003). Hence, zircon samples of higher concentration of uranium should exhibit a larger width of the peak at 1008 cm^{-1}, and such a correlation is in fact observed for Z1a and Z1b (Table. 1).

In Figure 3, a grain of zircon shows well-resolved zoning in the BSE image (sample Z2 from an equigranular metagranite). In the CL image, the sample appears dark owing to a high degree of structural disorder and a large amount of impurities, as detected by electron-microprobe analysis (Table 1). The Raman spectra collected from sample Z2 exhibit features revealing a high degree of structural damage: a broadening of the zircon peaks at 1008, 439 and 357 cm^{-1}, a change in the relative intensities of the stretching and bending modes of the SiO_4 units, and a number of additional peaks. These spectral peculiarities are more pronounced for the external zones Z2b and Z2c, which is related to the higher concentration of radioactive elements than in the internal zone Z2a. The overall broadening of the peaks generated by zircon modes points to a wide range in both the bond lengths and the bond angles, *i.e*., to a high degree of metamictization of the structure in this sample. The strong decrease in the relative intensity of $B_{1g}[\nu_3(SiO_4)]$ for Z2b and Z2c suggests a high degree of faults in the periodicity in the structure and, hence, fragmentation and misorientation of the crystalline domains. The appearance of a hump between 900 and 1200 cm^{-1} points to a substantial structural damage in Z2b and Z2c. The Raman scattering at 162, 509 and 635 cm^{-1} lies in the spectral range of the vibrational modes of Zr–O–Zr species, but the signals do not match strictly the Raman peaks of polymorphs of zirconia or zirconate phases (Zhang *et al*. 2000, Dobal & Katiyar 2002). Thus, we attribute these peaks to Zr-rich clusters of linked ZrO_n polyhedra or to the presence of a submicrometric non-crystalline Zr–O phase. The position of the extra Raman scattering at 785 cm^{-1} is close to the spectral range of the most intense Raman peaks of silicates containing quasi-isolated SiO_4 tetrahedra. Therefore, we suggest that this signal arises from Si-rich phases that are formed together with ZrO_n clusters as a result of the strong violation of the framework topology of zircon. The content of radioactive elements is lower in the internal zone Z2a and higher in the outer areas (Z2b and Z2c), thus indicating that radioactive decay is the major factor for the enhanced metamictization of the peripheral zones.

Figure 4 shows the BSE micrograph and the Raman spectra of sample Z3. According to the CL and BSE images, this grain of zircon possesses a core and an overgrowth. Because of the high content of U and the preserved zoning, both typical of crystal growth in a granitic melt, we assume that the rim of Z3 is of granitic origin, whereas the core is inherited. The Raman scattering reveals that the structure of the core (Z3a) is more ordered than that in the outermost zones. However, within the overgrown rim, one can distinguish two zones, Z3b and Z3c, differing from each other both in chemical composition and in Raman spectral features. The inner zone Z3b adjacent to the core has a higher content of U and a higher degree of metamictiza-

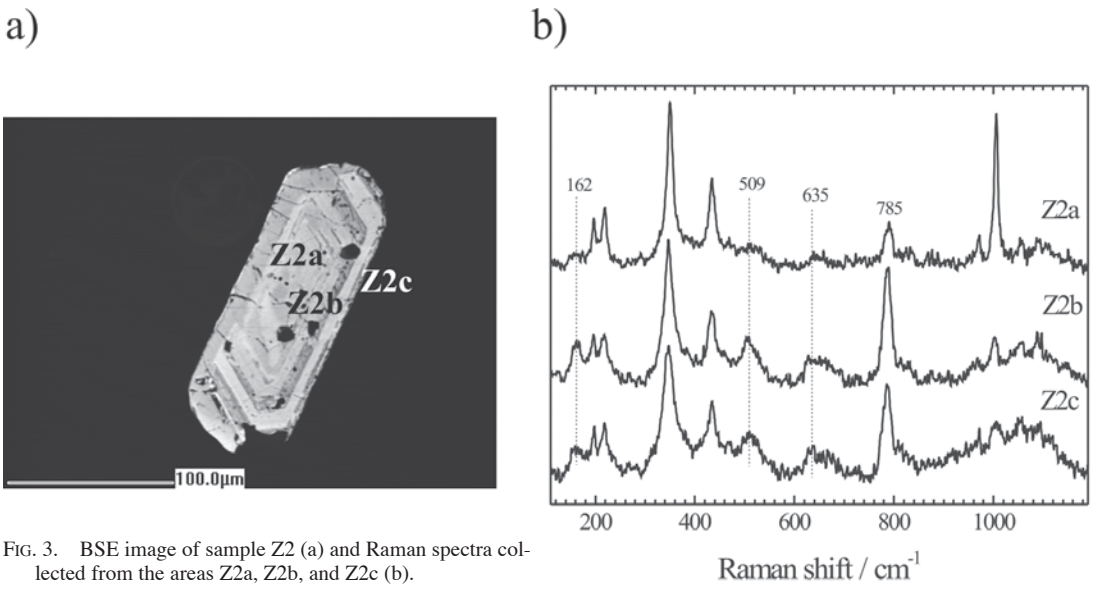

FIG. 3. BSE image of sample Z2 (a) and Raman spectra collected from the areas Z2a, Z2b, and Z2c (b).

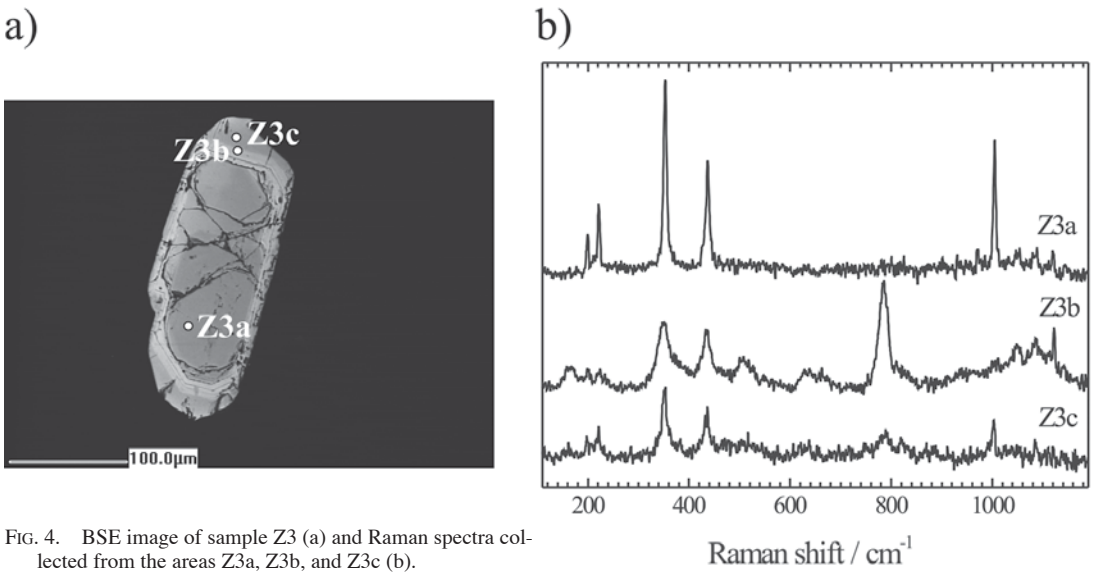

FIG. 4. BSE image of sample Z3 (a) and Raman spectra collected from the areas Z3a, Z3b, and Z3c (b).

tion. The structural state of Z3b resembles that of the peripheral zones of Z2: an extensive loss of periodicity, a wide range of the bond angles, and discrete Zr- and Si-rich domains. According to the Raman spectra, the structure of the outermost zone Z3c has a lower degree of metamictization than Z3b. At the same time, the electron-microprobe data show that Z3c is poor in U, a fact indicating the occurrence of recrystallization processes due to secondary heating.

Some of the investigated samples exhibit spectra in which the most intense Raman band is between 945 and 985 cm^{-1} (Fig. 5, bottom curve). This band consists of two relatively narrow components, with wavenumbers of 956 and 968 cm^{-1}, and FWHM values of 8 and 10 cm^{-1}, respectively. We assign the higher-energy component at 968 cm^{-1} to the symmetrical stretching mode of SiO_4 tetrahedra in the atomic environment of zircon, whereas we attribute the lower-energy signal at 956 cm^{-1} to perturbed Si–O bonds, *e.g.,* Si–OH species. Peaks arising from the antisymmetrical stretching, symmetrical bending and rotational mode of SiO_4 groups are seen at 1003, 438 and 352 cm^{-1}, respectively. These peaks are unusually weak compared to the Raman scattering near 968 cm^{-1}. It is worth noting that a broad Raman band near 962 cm^{-1} and a subtle scattering near 1006 cm^{-1} have been detected by Veytizou *et al*. (2000) in precursor gels for the synthesis of zircon. The latter has been attributed to the $B_{1g}[\nu_3(SiO_4)]$ zircon peak, whereas the former is attributed to Si–O–Zr bonds or Si–OH linkages (or both). Generally, the symmetrical stretching mode of an isolated TO_4 group generates the most intense Raman peak, and its suppression in crystalline matrices compared to the other internal tetrahedron modes results from constraints in the corresponding space-group symmetry. Thus, the high intensity of the zircon peak related to the $\nu_1(SiO_4)$ mode, compared to the other zircon peaks (near 1008, 439 and 357 cm^{-1}), indicates the prevalence of structural species in which the selection rules required by the zircon crystal-lattice symmetry have significantly deteriorated. We propose that the structure of the samples, exhibiting atypical Raman scattering, with the most intense bands at 956 and 968 cm^{-1}, consists of incipient grains of zircon of a very small size, with OH groups on the intergranular interface. This assumption is supported by the observed laser-induced spectral changes (Fig. 5). An increase in laser power leads to the disappearance of the peak at 956 cm^{-1} and to an increase in the relative intensity of the zircon peak arising from the $B_{1g}[\nu_3(SiO_4)]$, $A_{1g}[\nu_2(SiO_4)]$ and $E_g[\mathrm{rot}(SiO_4)]$ modes. The former effect indicates a removal of OH groups, whereas the latter is indicative of the development of the zircon structure. Obviously, the laser irradiation leads to local heating, which enhances the growth of the zircon nuclei. Thus the atypical Raman scattering with an intensified symmetrical SiO_4 stretching mode points to the presence of incipient zircon species, *i.e.,* to a structural state of incipient recrystallization. Among the zircon grains investigated, those from porphyritic granites and melanocratic enclaves possess such a Raman spectrum. These grains are relatively homogeneous in structure, as revealed by Raman microspectroscopy and CL textural features. As the zircon grains considered are separated from strongly deformed samples, one can suggest that the structural state of zircon is a result of a structural alteration related to fluid activity.

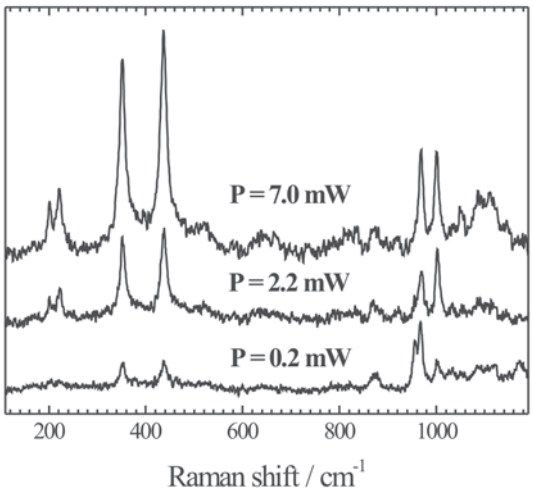

FIG. 5. Raman spectra collected from the same zone in a zircon grain (Z4) with different laser powers applied. A laser power of 0.2 mW at the sample surface was found to be low enough for non-destructive measurements. The CL image of sample Z4 is dark, without any differences in the contrast; no differences in Raman scattering collected from different spatial areas with the same laser power were detected.

DISCUSSION

According to their Raman spectral features, the spatial regions in the zircon samples can be divided into two groups: (A) regions with well-resolved Raman scattering near 1008 cm^{-1}, and (B) regions with very weak Raman scattering near 1008 cm^{-1}, pointing to a highly disordered state of zircon.

The latter group (B) can further be divided into two subgroups depending on the internal textures and chemical composition. The B-i subgroup shows dark areas in CL images, with high concentrations of uranium (up to 7000 ppm); the high concentrations of U and Th confirm that radiation damage is the main factor causing the observed structural damage. Subgroup B-ii shows bright areas in CL, with a low concentration of U and Th, but with a high level of structural damage; such zones usually are external rims, suggesting the occurrence of subsequent chemical alteration and migration of uranium.

The degree of metamictization is commonly determined on the basis of the FWHM of the $B_{1g}([\nu_3(SiO_4)]$ mode, giving rise to the peak near 1008 cm^{-1} (Nasdala *et al*. 1995, Palenik *et al*. 2003). There is a linear correlation between the width and the position of this peak for those areas in group A that exhibit resolved Raman scattering near 1008 cm^{-1} (Fig. 6a). These areas contain intermediate concentrations of uranium (~350–2000 ppm). The FWHM ranges between 3 and 10 cm^{-1}. Thus

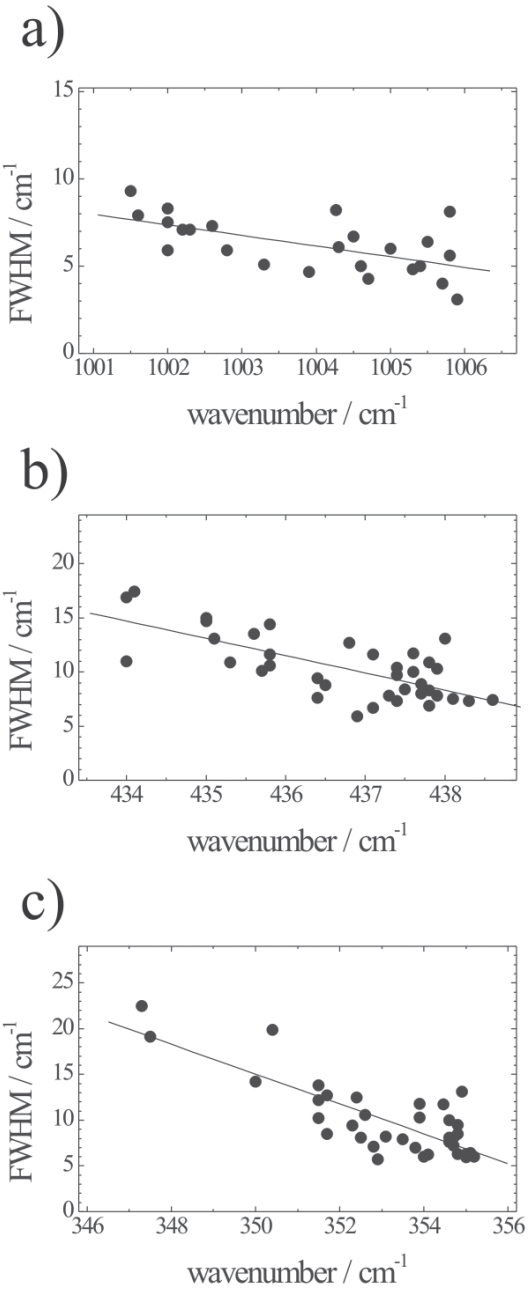

FIG. 6. Peak width *versus* peak position of the Raman signals near 1008 (a), 439 (b) and 357 cm^{-1} (c). The spectral parameters were determined by fitting the spectrum profile with Lorentzians, and the measured FWHM were subsequently corrected for the apparatus function according to Irmer (1985). The lines represent the linear fits of the experimental data.

the degree of metamictization varies from well-ordered crystalline to an intermediate metamict state (Nasdala *et al*. 1995). However, the FWHM of the peaks are narrower than expected for unannealed primary zircon (Geisler *et al*. 2001). This anomaly is more pronounced for the peaks shifted to the lower wavenumbers (down to 1001 cm^{-1}). Such a dependence has been reported by Geisler *et al*. (2001) for experimentally annealed zircon. They observed two stages of recovery characterized by regression lines of different slope and a relatively low dependence of the peak position on FWHM for the higher-temperature recovery stage. Thus the large dispersion of data points in Figure 6a can be explained by different initial accumulation of structural damage and to various thermal histories among the zircon crystals in the present study.

In addition, we considered the correlation of the FWHM with the position of the peaks near 439 and 357 cm^{-1}, derived from the modes $A_{1g}[\nu_2(SiO_4)]$ and $E_g[rot(SiO_4)]$, respectively (Figs. 6b, c). The experimental data were fitted using the function $\Gamma = \Gamma_0 - k.\omega$, where Γ and ω stand for FWHM and peak position, respectively, whereas k gives the line slope, which turns out to be approximately the same for the two modes, namely $k = 1.62 \pm 0.25$ ($R^2 = 0.75$) for $A_{1g}[\nu_2(SiO_4)]$ and $k = 1.58 \pm 0.20$ ($R^2 = 0.80$) for $E_g[rot(SiO_4)]$. Well-pronounced Raman signals near 439 and 357 cm^{-1} were detected for all the samples studied, regardless of the degree of metamictization. Because of the type of generating modes (SiO_4 bending and rotation), these peaks are indicative of the existence of ZrO_8–SiO_4 linkages characteristic of zircon. Therefore, the peaks at 439 and 357 cm^{-1} are representative of zircon-type medium-range order and can also be used to estimate the degree of metamictization in cases where there is not a pronounced Raman peak at 1008 cm^{-1}. Further investigations of the diversity of zircon samples are necessary to clarify the relationship between these peaks and the degree of structural damage.

Conclusions

The structural state of micrometric areas in heterogeneous grains of zircon was estimated on the basis of the Raman scattering in the spectral range 50–1250 cm^{-1} as follows: 1) a spectrum differing from that of well-crystalline synthetic zircon only in position and width of the 1008 cm^{-1} peak reveals a variation in the Si–O bond lengths; 2) a substantial decrease in the intensity of the phonon mode B_{1g}, related to the antisymmetrical stretching mode $\nu_3(SiO_4)$, points to a nanoscale misorientation of the zircon crystallites and a partial loss of periodicity; 3) the appearance of additional Raman scattering near 162, 509 and 635 cm^{-1} reveals clustering of ZrO_n polyhedra, whereas extra Raman scattering near 785 cm^{-1} can be attributed to Si-rich domains. Substantial broadening of the peaks near 357 and 459 cm^{-1} indicates a large range in the Zr–O–Si bond angles; 4) the enhanced two-component band between 945 and 985 cm^{-1} related to $\nu_1(SiO_4)$ speaks in favor of an abundance of incipient grains of zircon.

The well-pronounced Raman peaks at 357 and 439 cm^{-1}, originating from SiO_4 rotational and bending modes, respectively, are sensitive to the structural state of zircon and may be used to estimate the degree of metamictization of zircon.

For most of the zircon samples considered in the present study, the degree of metamictization varies even within a single grain, suggesting that the recrystallization processes had not been strong enough to ensure a complete recovery of the damaged structure. The grains from equigranular metagranites show a broad range of structural variations: (i) zones exhibiting peak positions and values of FWHM close to those of synthetic crystalline zircon; (ii) zones for which the $B_{1g}[\nu_3(SiO_4)]$ peak has small FWHM (5–8 cm^{-1}), but is positioned at anomalously low wavenumbers (1003–1001 cm^{-1}); (iii) zones characterized by a low-intensity or missing peak at 1008 cm^{-1} and by the appearance of additional non-zircon Raman peaks.

Samples separated from highly migmatized rocks show chemical, textural and structural homogeneity. They show a low-intensity peak near 1008 cm^{-1} and instability to high-power laser irradiation. These structural characteristics most probably result from a strong secondary alteration in the presence of a fluid phase.

Acknowledgements

We acknowledge the support of the European Community Access to Research Infrastructure action of the Improving Human Potential Programme, contract HPRI–CT–1999–00008 awarded to Prof. B.J. Wood (EU Geochemical Facility, University of Bristol) for electron-microprobe analysis and BSE images. We thank Dr. Bernd Güttler, PTB–Braunschweig, for enabling the Raman spectroscopic measurements in his laboratory. Financial support from the National Science Fund – Bulgarian Ministry of Education and Science (F1212 and NT 1–02) is gratefully acknowledged. Thanks are due to referees S. Utsonomiya and N. Tomasic, and to R.F. Martin, for their constructive suggestions and valuable comments.

References

Benisek, A. & Finger, F. (1993): Factors controlling the development of prism faces in granite zircons: a microprobe study. *Contrib. Mineral. Petrol.* **114**, 441-451.

Dawson, P., Hargreave, M.M. & Wilkinson, G.R. (1971): The vibrational spectrum of zircon ($ZrSiO_4$). *J. Phys. C: Solid State Phys.* **4**, 240-256.

Dobal, P.S. & Katiyar, R.S. (2002): Studies on ferroelectric perovskites and Bi-layered compounds using micro-Raman spectroscopy. *J. Raman Spectros.* **33**, 405-423.

EWING, R.C., LUTZE, W. & WEBER, W.J., (1995): Zircon: a host-phase for the disposal of weapons plutonium. *J. Mater. Res.* **10**, 243-246.

EWING, R.C., MELDRUM, A., WANG, L.M. & WANG, S.X. (2000): Radiation-induced amorphization. *In* Transformation Processes in Minerals (S.A.T. Redfern & M.A. Carpenter, eds.). *Rev. Mineral. Geochem.* **39**, 319-361.

EWING, R.C., MELDRUM, A., WANG, L., WEBER, W.J. & CORRALES, L.R. (2003): Radiation effects in zircon. *In* Zircon (J.M. Hanchar & P.W.O. Hoskin, eds.). *Rev. Mineral. Geochem.* **53**, 387-425.

GEISLER, T. & PIDGEON, R. (2001): Significance of radiation damage on the integral SEM cathodoluminescence intensity of zircon: an experimental annealing study. *Neues Jahrb. Mineral., Monatsh.*, 433-445.

GEISLER, T. & PIDGEON, R.T. (2002): Raman scattering from metamict zircon: comments on "Metamictisation of natural zircon: accumulation versus thermal annealing of radioactivity-induced damage " by Nasdala *et al.* (*Contrib. Mineral. Petrol.* **141**, 125-144). *Contrib. Mineral. Petrol.* **143**, 750-755.

GEISLER, T., PIDGEON, R., KURTZ, R., VAN BRONSWIJK, W. & SCHLEICHER, H. (2003a): Experimental hydrothermal alteration of partially metamict zircon. *Am. Mineral.* **88**, 1496-1513.

GEISLER, T., PIDGEON, R., VAN BRONSWIJK, W. & PLEYSIER, R. (2001): Kinetics of thermal recovery and recrystallization of partially metamict zircon: a Raman spectroscopic study. *Eur. J. Mineral.* **13**, 1163-1176.

GEISLER, T., ZHANG, MING, SALJE, E.K.H. (2003b): Recrystallization of almost fully amorphous zircon under hydrothermal conditions: an infrared spectroscopic study. *J. Nucl. Mater.* **320**, 280-291.

HANCHAR, J.M. & RUDNICK, R.L. (1995): Revealing hidden structures: the application of cathodoluminescence and backscattered electron imaging to dating zircon from lower crustal xenoliths. *Lithos* **36**, 289-303.

HOLLAND, H.D. & GOTTFRIED, D. (1955): The effect of nuclear radiation on the structure of zircon. *Acta Crystallogr.* **8**, 291-300.

HOSKIN, P.W.O. & BLACK, L.P. (2000): Metamorphic zircon formation by solid-state recrystallization of protolith igneous zircon. *J. Metam. Geol.* **18**, 423-439.

IRMER, G. (1985): Zum Einfluß der Apparatefunktion auf die Bestimmung von Streuquerschnitten und Lebensdauern aus optischen Phononenspektren. *Exp. Techn. Physik* **33**, 501-506.

KOLESOV, B.A., GEIGER, C.A. & ARMBRUSTER, T. (2001): The dynamic properties of zircon studied by single-crystal X-ray diffraction and Raman spectroscopy. *Eur. J. Mineral.* **13**, 939-948.

NASDALA, L., BERAN, A., LIBOWITZKY, E. & WOLF, D. (2001b): The incorporation of hydroxyl groups and molecular water in natural zircon ($ZrSiO_4$). *Am. J. Sci.* **301**, 831-857.

NASDALA, L., IRMER, G. & WOLF, D. (1995): The degree of metamictization in zircon: a Raman spectroscopic study. *Eur. J. Mineral.* **7**, 471-478.

NASDALA, L., LENGAUER, C.L., HANCHAR, J.M., KRONZ, A., WIRTH, R., BLANC, P., KENNEDY, A.K. & SEYDOUX-GUILLAUME, A.-M. (2002): Annealing radiation damage and the recovery of cathodoluminescence. *Chem. Geol.* **191**, 121-140.

NASDALA, L., WENZEL, M., VAVRA, G., IRMER, G., WENZEL, T. & KOBER, B. (2001a): Metamictisation of natural zircon: accumulation versus thermal annealing of radioactivity-induced damage. *Contrib. Mineral. Petrol.* **141**, 125-144.

NASDALA, L., ZHANG, M., KEMPE, U., PANCZER, G., GAFT, M., ANDRUT, M. & PLÖTZE, M. (2003): Spectroscopic methods applied to zircon. *In* Zircon (J.M. Hanchar & P.W.O. Hoskin, eds.). *Rev. Mineral. Geochem.* **53**, 427-467.

PALENIK, C.S., NASDALA, L. & EWING, R.C. (2003): Radiation damage in zircon. *Am. Mineral.* **88**, 770-781.

PIDGEON, R.T. (1992): Recrystallization of oscillatory zoned zircon: some geochronological and petrological implications. *Contrib. Mineral. Petrol.* **110**, 463-472.

SCHALTEGGER, U., FANNING, C.M., GÜNTER, D., MAURIN, J.C., SCHULMANN, K. & GEBAUER, D. (1999): Growth, annealing and recrystallization of zircon and preservation of monazite in high-grade metamorphism: conventional and in-situ U–Pb isotope, cathodoluminescence and microchemical evidence. *Contrib. Mineral. Petrol.* **134**, 186-201.

SYME, R.W.G., LOCKWOOD, D.J. & KERR, H.J. (1977): Raman spectrum of synthetic zircon ($ZrSiO_4$) and thorite ($ThSiO_4$). *J. Phys. C: Solid State Phys.* **10**, 1335-1348.

TITORENKOVA, R., MACHEVA, L., ZIDAROV, N., VON QUADT, A. & PEJTCHEVA, I. (2003): Metagranites from SW Bulgaria as a part of the Neoproterozoic to early Paleozoic system in Europe: new insight from zircon typology, U–Pb isotope data and Hf-tracing. *Geophys. Res. Abstr.* **5**, 08963.

TRACHENKO, K., DOVE, M.T. & SALJE, E.K.H. (2002): Structural changes in zircon under α-decay irradiation. *Phys. Rev. B* **65**, 180102-1 – 180102-3.

VAVRA, G., SCHMID, R. & GEBAUER, D. (1999): Internal morphology, habit and U–Th–Pb microanalysis of amphibolite-to-granulite facies zircon: geochronology of the Ivrea zone (southern Alps). *Contrib. Mineral. Petrol.* **134**, 380-404.

VEYTIZOU, C., QUINSON, J.-F. & DOUY, A. (2000): Sol–gel synthesis *via* an aqueous semi-alkoxide route and characterization of zircon powders. *J. Mater. Chem.* **10**, 365-370.

ZHANG, MING, SALJE, E.K.H., CAPITANI, G.C., LEROUX, H., CLARK, A.M., SCHLÜTER, J. & EWING, R.C. (2000): Annealing of α-decay damage in zircon: a Raman spectroscopic study. *J. Phys.: Condens. Matter* **12**, 3131-3148.

Received March 15, 2006, revised manuscript accepted June 8, 2006.